ELSEVIER

Finite Elements in Analysis and Design 37 (2001) 365–380

FINITE ELEMENTS IN ANALYSIS AND DESIGN

www.elsevier.com/locate/finel

Viscous single and multicomponent airfoil design with genetic algorithms

D. Quagliarella*, A. Vicini

C.I.R.A., Centro Italiano Ricerche Aerospaziali, Via Maiorise, 81043 Capua, Italy

Abstract

An optimization procedure aimed at the design of multicomponent airfoils for high-lift applications is described. The procedure is based on a multiobjective genetic algorithm; two flow solvers have been coupled with the genetic algorithm: a viscous–inviscid interaction method, based on an Euler flow solver and an integral boundary layer routine, and a method based on a full potential flow solver. The first model is used for high-lift configurations, whereas the second is used to optimize transonic performances for cruise configurations. The applications described include both single and multiobjective design of a high-lift multicomponent airfoil, and a multipoint design where the transonic and high-lift requirements are taken into account simultaneously.

Keywords: Multiobjective optimization; Multi-point design; High-lift; Genetic algorithms; Multielement airfoils

1. Introduction

The goal of the aerodynamic design of a wing for a transport aircraft is to minimize the drag in cruise condition, while satisfying constraints on lifting force, pitching moment and wing structure requirements. The main goal of a high-lift system, on the other hand, is the maximization of lift; in this case, the objective of the aerodynamic design is to achieve maximum lift without massive flow separation [1].

When numerical optimization is used to approach the design problem, the reliability of the results that can be obtained is the same of the aerodynamic analysis models that are used. Common cruise conditions are in the transonic regime, and the main contribution to drag comes from the generated shock waves. Therefore, from a numerical point of view, a non-viscous flow field solver that can compute the drag contribution due to weak shock waves is an adequate tool to provide the

* Corresponding author.

0168-874X/01/$ - see front matter
PII: S0168-874X(00)00053-6

information needed by an optimization procedure, provided that there is not extensive flow separation. On the contrary, high-lift flows are characterized by many complex features, such as different transition phenomena on each of the airfoil elements, confluence of wakes into boundary layers, regions of separated flows etc., that make their prediction through numerical simulation a very challenging task. Therefore an inviscid analysis, although useful for a rough estimation of pressure distributions, does not provide enough information for a reliable design. Besides, it has to be pointed out that even the most advanced CFD technology shows serious limits in the evaluation of such a kind of flows, and therefore the results obtained by any numerical optimization process have to be verified through experiments [2].

In the present work a multi-point design optimization method has been developed for transonic and high-lift airfoil configurations. The method builds up on a multiobjective genetic algorithm coupled to two different flow field solvers. It is a direct method, as the global flow field characteristics – such as wave drag in transonic regime and lift force in high-lift conditions – are directly addressed as design objectives.

The flow field around the single-element airfoil in cruise conditions is evaluated through a full potential approximation of the Navier – Stokes equations, solved using a finite difference scheme. High-lift flow is evaluated, instead, using an Euler/boundary layer interaction method.

The developed system is capable of taking into account transonic and high-lift requirements at the same time through multiobjective optimization. As anticipated, the optimization tool adopted to this purpose is a genetic algorithm. The main reason for this choice is that these algorithms offer an easy and straightforward implementation of multiobjective optimization. Furthermore, they do not require evaluation of gradients, which can be a difficult task, when one has to deal with turbulent and separated flows, as the aerodynamic analysis is subject to convergence problems and even failures. From this point of view, a gradient-free approach to optimization offers a much more robust environment. On the other hand, it must be pointed out that computational efficiency of genetic algorithms is inferior to classical gradient-based methods, and their use is convenient only when classical techniques show their limits.

2. The multiobjective genetic algorithm

As anticipated the optimization tool described in this work is based on a multiple-objective genetic algorithm [3,4,11].

Direct multiobjective optimization may be particularly useful when several conflicting requirements have to be satisfied at the same time. In fact, the given set of objective functions is optimized without the need of being arbitrarily combined. In other words, it is not necessary to assign arbitrary weights to combine different design objectives into a single one, which may be tricky especially when the design objectives are of different nature. From this point of view, this approach radically differs from more usual ones, which are only able to deal with scalar objectives functions.

From a conceptual point of view, the main difference between single- and multiple-objective optimization is the definition of optimal solution, that is an extension of the single-objective optimum concept.

A feasible solution to a multiobjective optimization problem is said optimal, or non-dominated, if, starting from that point in the design space, the value of any of the objective functions cannot be improved without deteriorating at least one of the others.

Pareto, a prominent Italian economist, introduced this idea of optimality at the end of the past century. To define the notion of domination let $\boldsymbol{f} = (f_1, \ldots f_n)$ and $\boldsymbol{g} = (g_1, \ldots, g_n)$ be two real-valued vectors of n elements; $\boldsymbol{f}$ is partially less than $\boldsymbol{g}$ (in symbols $\boldsymbol{f} <_{\mathrm{p}} \boldsymbol{g}$) if

$$\forall i \in (1, \ldots, n) \quad f_i \leqslant g_i \quad \text{and} \quad \exists i: \quad f_i < g_i \tag{1}$$

If $\boldsymbol{f} <_{\mathrm{p}} \boldsymbol{g}$, we say that $\boldsymbol{f}$ dominates $\boldsymbol{g}$. Consequently, a feasible solution $\boldsymbol{x}^*$ is said a Pareto optimal if and only if it does not exist another feasible solution $\boldsymbol{x}$ such that $\boldsymbol{f}(\boldsymbol{x}) <_{\mathrm{p}} \boldsymbol{f}(\boldsymbol{x}^*)$.

From the previously given definition of optimality it follows that, in general, the optimal solution to a multiobjective problem is not unique. All feasible solutions can, indeed, be classified into dominated and non-dominated (Pareto optimal) solutions, and the set of non-dominated solutions is called Pareto front. Solving a multiobjective optimization problem is therefore, to find this set or to approximate it with a representative subset. Afterwards the decision-maker's preference may be applied to choose the best compromise solution from the generated set.

A genetic algorithm can use the above defined dominance criteria in a straightforward fashion, to drive the evolution of the population towards the Pareto front [5].

In this work this has been accomplished by selecting the elements appointed for reproduction using a random walk operator. The basic difference with respect to a single-objective algorithm is that, in this case, the elements selected are not the best fit ones, but the locally non-dominated among those met in the walk. If more non-dominated solutions are met, the first one encountered is selected. At the end of every new generation, the set of Pareto optimal solutions is updated and stored.

A sort of extension of the elitism strategy to multiobjective optimization can also be adopted by randomly selecting an assigned percentage of parents from the current set of non dominated solutions.

3. Aerodynamic flow solvers

Two different flow field solvers have been used in this optimization procedure. The single-element airfoil in cruise conditions is, in fact, optimized for wave drag, and to that purpose a full potential transonic flow field solver, with non conservative formulation, is considered adequate to compute the flow field [6].

In high-lift conditions the flow field is computed, instead, through a semi-inverse viscous/inviscid coupling technique [7]. The inviscid part of the flow field is modeled using the Euler equations written in integral form. The equation system is solved numerically using the finite-volume scheme introduced by Jameson et al. [8]. Integral compressible boundary layer equations are then used to calculate the viscous flow. The direct formulation of the boundary layer equations is used for attached flow regions, while separated flow zones are solved using the inverse form of these equations. The boundary layer influence on the external flow is simulated through the Lightill's 'equivalent sources' concept [9]. Following this approach, the thickening of the body, due to the boundary layer displacement thickness, is equivalent to a surface distribution of sources. During viscous/inviscid interaction these sources are used as boundary conditions on the original body in the solution of the inviscid equations.

4. Airfoil shape parameterization

One of the critical points of multielement airfoil design is geometry parameterization and handling. In fact, correspondence must be ensured between the clean configuration for transonic cruise and the high-lift multielement one.

This can be achieved in various ways, each with different advantages and shortcomings. The usual approach is to perform separately the clean configuration design, which must be optimized for transonic cruise, and the high-lift one. In this case, the single-element configuration can be changed using classical approaches like *b*-spline or modification functions [3]. In a second step, the flap, slat and cove portions that do not introduce changes in the clean configurations can be modified, along with their relative positions, when the airfoil is optimized for high-lift performances. Alternatively, if the possible interactions between cruise and high-lift configurations have to be explored, it may be more convenient to face the problem in a multiobjective fashion, by modifying single- and multielement configuration at the same time.

In the present work single-point design applications of an airfoil high-lift configuration will be shown, also including the modification of the main body shape; both single and multiobjective approaches are used. Afterwards, the previously described multi-point design is illustrated by taking into account transonic and high-lift requirements at the same time.

Analytically defined modifications functions are used for the airfoil shape modification. The airfoil shape is thus defined as

$$y(x) = y_0(x) + \sum_{i=1}^{n} w_i f_i(x), \tag{2}$$

where $y_0(x)$ is the initial geometry, $f_i(x)$, $i = 1, \ldots, n$, is the modification function set, and w_i are the design variables. The modification functions can be defined so as to modify the entire airfoil, or only a specified part of it. In the single-point design examples only the airfoil portion that does not belong to the high-lift devices is changed. On the other hand, in the multi-point design the whole airfoil shape is changed. Consequently, also the parts of the high-lift configuration such as flap nose and slat cove must be changed to ensure geometry coherency.

To this purpose, in the present work, the following approach has been used. Let $y_u(x)$ and $y_\ell(x)$ be the upper and lower surface ordinates of the single-element airfoil, and $dy_u(x)$ and $dy_\ell(x)$ their respective modifications. Let now $y_u^f(x)$ and $y_\ell^f(x)$ be the flap ordinates in its closed position. We introduce the following linear blending functions:

$$b_u(x) = \frac{y_u(x) - y_u^f(x)}{y_u(x) - y_\ell(x)}, \tag{3}$$

and

$$b_\ell(x) = \frac{y_u(x) - y_\ell^f(x)}{y_u(x) - y_\ell(x)}, \tag{4}$$

then the upper flap shape modification is obtained as

$$\mathrm{d}y_u^f(x) = b_u(x)\,\mathrm{d}y_u(x) + (1 - b_u(x))\,\mathrm{d}y_\ell(x) \tag{5}$$

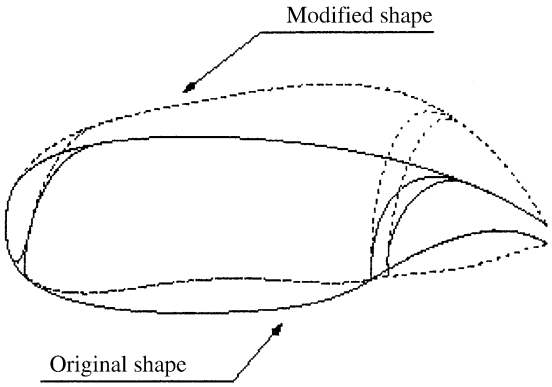

Fig. 1. Modification of the airfoil and its high-lift devices.

and for the lower flap surface:

$$\mathrm{d}y_\ell^{\mathrm{f}}(x) = b_\ell(x)\,\mathrm{d}y_{\mathrm{u}}(x) + (1 - b_\ell(x))\,\mathrm{d}y_\ell(x). \tag{6}$$

As can be observed in Fig. 1, this kind of modification ensures that the wetted portions of the high-lift devices (slat, flap, etc.) coincide with the modified airfoil shape, while their 'internal' portions guarantee the necessary geometric conditions.

5. Optimization examples

Four different optimization runs have been performed each starting from the same clean configuration. The problem parameters are the relative position and rotation of flap and slat (when present), and the shape of the airfoils components. Flap and slat rotate around their leading edge; positive rotation is counterclockwise.

Two design points are prescribed at Mach 0.20 for high-lift configurations and Mach 0.85 for transonic cruise configurations, while Reynolds number is fixed to 8 000 000.

In first point, relative to the high-lift configuration, lift force maximization is required, with or without constraint on pitching moment. The objective function to be minimized is therefore

$$1/c_\ell^2. \tag{7}$$

The pitching moment is controlled through the introduction of an auxiliary objective function to be minimized that is

$$k(c_{\mathrm{m}} - \underline{c}_{\mathrm{m}})^2, \tag{8}$$

where $\underline{c}_{\mathrm{m}} = -0.27$ and k has been set to 200.

The angle of attack, at which the configuration has to be optimized, is chosen to be 5°.

The second design point is relative to the clean configuration, and the minimization of the wave-drag coefficient c_{dw} is required at $c_\ell = 0.5$. The objective function is therefore

$$kc_{\mathrm{dw}} \tag{9}$$

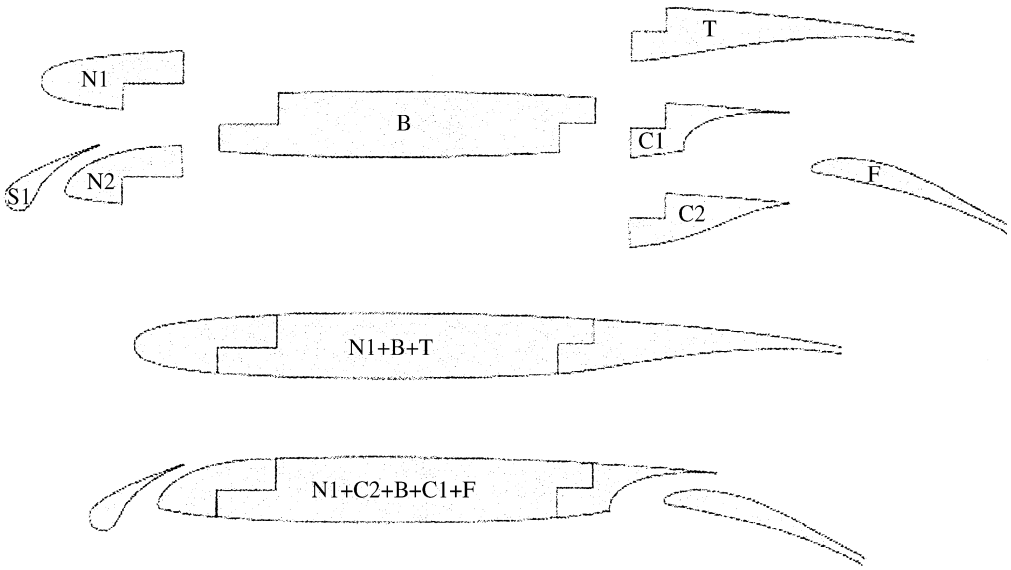

Fig. 2. Components of the initial airfoil shape.

with $k = 400$ in each run. The angle of attack of the airfoil is changed in order to satisfy explicitly the constraint on lift coefficient. A constraint is imposed on the maximum thickness of the airfoil:

$$t = 9.7\%. \tag{10}$$

This constraint is explicitly satisfied by scaling the airfoil to the given thickness.

5.1. Initial configuration

The initial configuration used for the high-lift and transonic runs was chosen from [10], where an airfoil, that is easily configurable for high-lift and transonic conditions, is used for wind tunnel tests. Fig. 2 reports some of the components of the airfoil system as well two examples of configurations. Each airfoil is formed by a main body (B) that can have different noses (N1, N2) and tails (T) or coves (C1, C2) attached. Nose N2 can be coupled to a slat (S1), and coves C1 and C2 can be coupled to a flap (F) that in its closed position corresponds to tail T.

The N1 + B + T configuration was chosen as base airfoil for the transonic single-element design point of the optimization runs reported here. Configurations N1 + B + C1 + F and S1 + N2 + B + C1 + F were instead used for high-lift design points.

5.2. Application example 1: c_ℓ maximization at $M = 0.2$ with a two-component airfoil

The first example reported is on the high-lift design point and the lift force is maximized without considering the effect on pitching moment. The allowed flap rotation range with respect to its closed position is $[-25, 0]$ deg. Flap translation ranges are $[0.03, 0.08]$ in x direction and [0.0, 0.025] in y direction; translation is considered with respect to flap closed position. Airfoil shape modification is allowed only on the upper surface of the main body.

Table 1
Modification functions used in the application example 1

Hicks–Henne functions	Legendre functions
$0.888(1-\xi)\sqrt{\xi}e^{-13.28\xi}$	$0.42(1-\xi)^3\sqrt{\xi}$
$0.57(1-\xi)\sqrt{\xi}e^{-5\xi}$	$0.946(1-\xi)^3\xi$
$0.1\sin^3(\pi\xi^{0.431})$	$0.136(1-\xi)^3(12\xi-10\xi^2)$
$0.1\sin^3(\pi\xi^{0.757})$	$(1-\xi)^3(225\xi-630\xi^4+560\xi^3-220\xi^3+30\xi)$
$0.1\sin^3(\pi\xi^{1.357})$	
$0.1\sin^3(\pi\xi^{3.106})$	

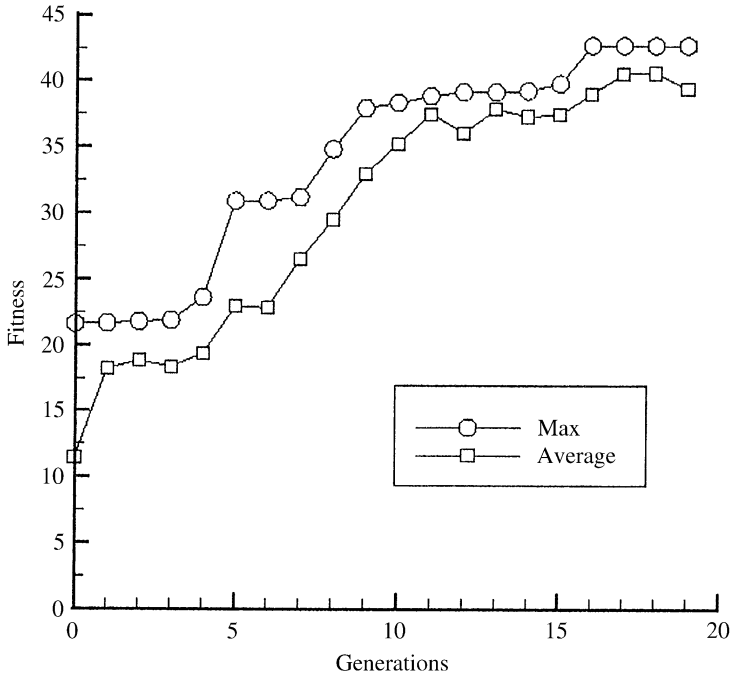

Fig. 3. Evolution history of the c_ℓ maximization test case without control on c_m.

Ten modification functions are applied between $x/c \in [0, 0.7]$. Letting $\xi = x(0.7/c)$, these functions are reported in Table 1.

A population of 20 individuals evolved for 20 generations; 8 bits were used for variable encoding; mutation at bit level with a probability of 2% and extended intermediate crossover [3] with 100% activation probability were used. Fig. 3 reports the evolution history of the fitness during the optimizing run.

The lift coefficient of the best individual is $c_\ell = 2.56$, and the corresponding pitching moment is $c_m = -0.43330$. Figs. 4 and 5 report the comparison between original and optimized pressure coefficients and airfoil shape, respectively.

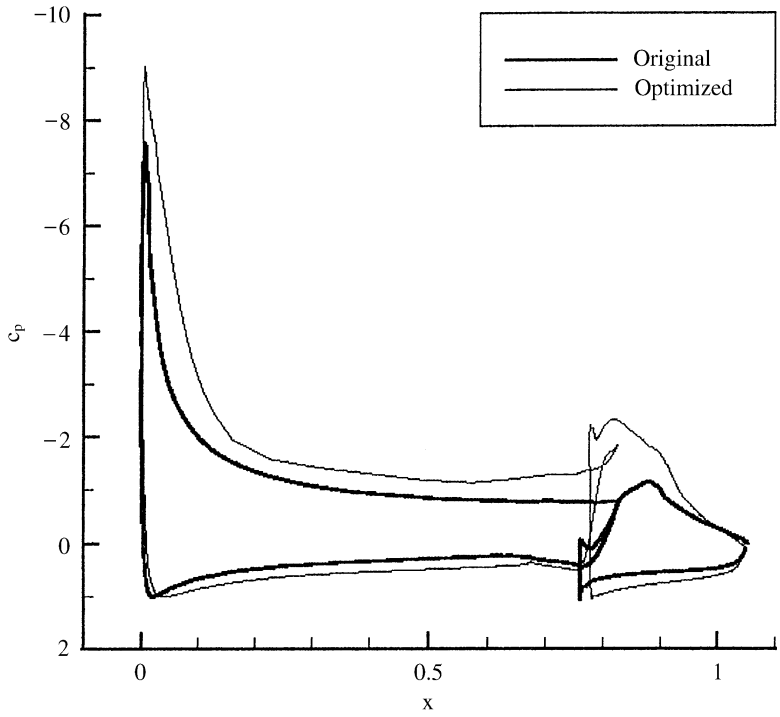

Fig. 4. c_p comparison for the application example 1.

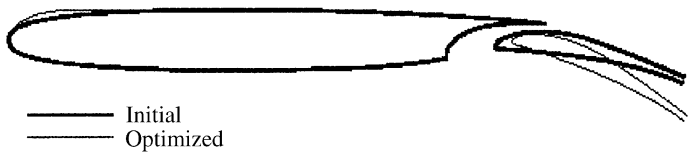

Fig. 5. Airfoil comparison for the application example 1.

5.3. *Application example 2*: c_ℓ *maximization at* $M = 0.2$ *with three-component airfoil*

This example solves the same single-objective problem of #1, but introduces a leading edge slat instead of changing the main body shape using modification functions. Therefore, only six design variables control the configuration. The allowed slat rotation range with respect to its closed position is $[-5, 5]$ degrees. Slat translation ranges are $[0.03, 0.08]$ in the x direction and $[-0.02, 0.02]$ in the y direction; translation is considered with respect to closed position. Flap allowed rotation and translation ranges are the same than problem #1.

A population of 20 individuals evolved for 30 generations; 8 bits were used for variable encoding; mutation at bit level with a probability of 10% and classical one-point crossover with 100% activation probability were used. Fig. 6 reports the evolution history of the lift coefficient during the optimization run, while the comparison of original and final pressure coefficients and airfoil shapes are reported in Figs. 7 and 8, respectively.

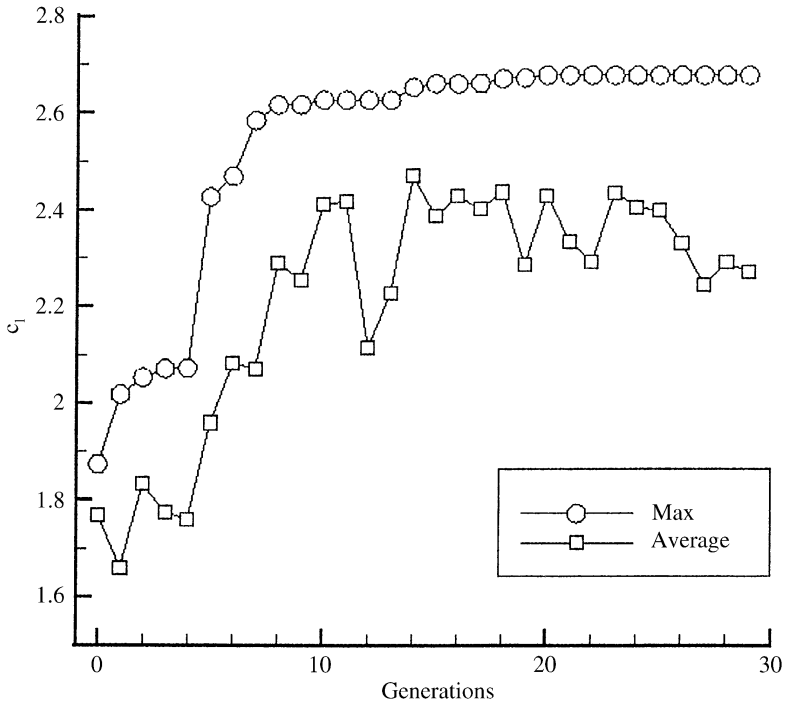

Fig. 6. c_ℓ evolution history for application example 2.

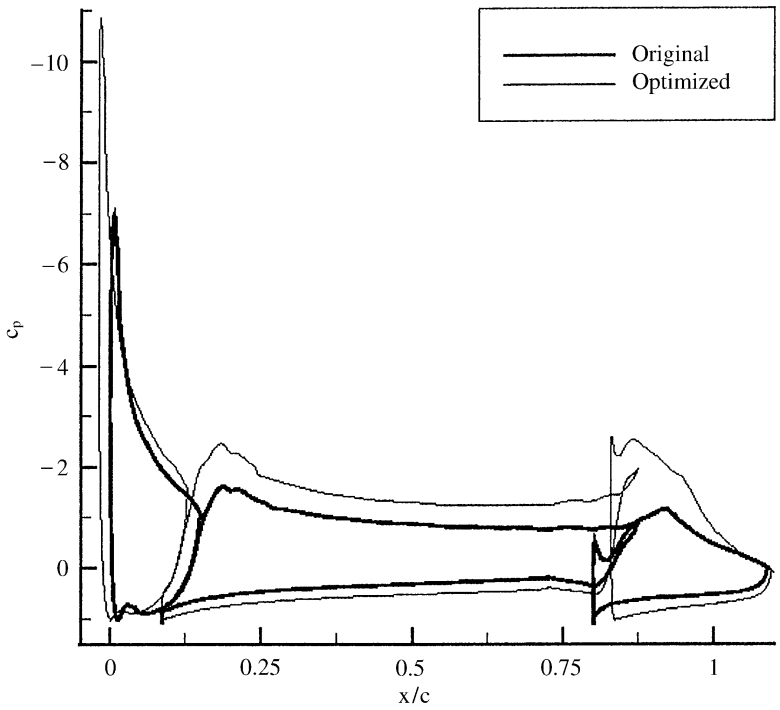

Fig. 7. c_p comparison for the application example 2.

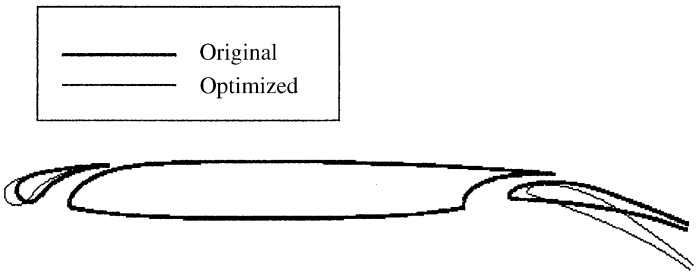

Fig. 8. Airfoil comparison for example 2.

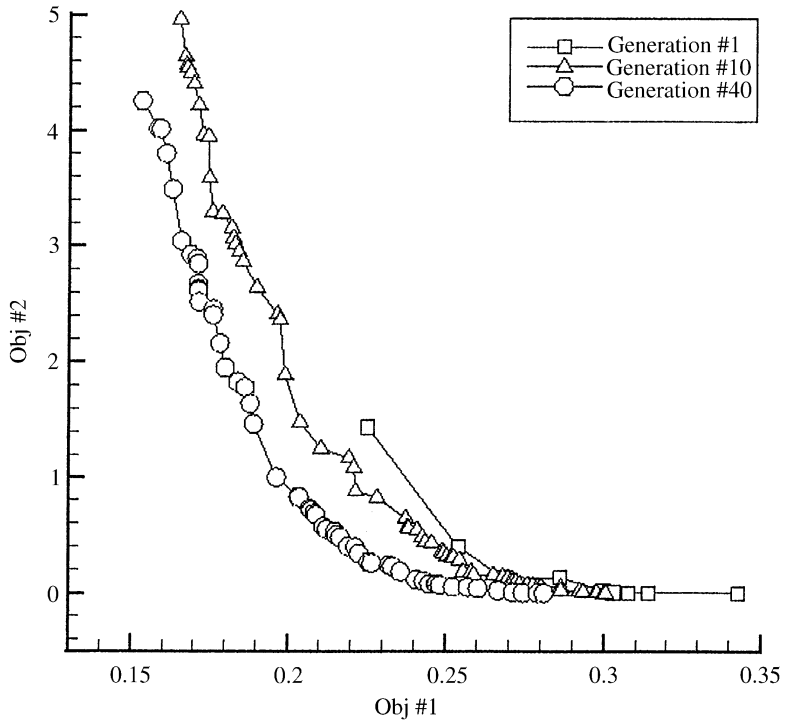

Fig. 9. Final and intermediate Pareto fronts for application 3.

5.4. Application example 3: c_ℓ maximization at $M = 0.2$ with a two-component airfoil and control on pitching moment

A population of 32 individuals evolved for 40 generations; 8 bits were used for variable encoding; mutation at bit level with a probability of 2% and extended intermediate crossover with 100% activation probability were used. Fig. 9 reports the final Pareto front and some intermediate ones. An airfoil belonging to the middle part of the final front was chosen and the comparison of its c_p distribution and shape with respect to the original configuration are reported in Figs. 10 and 11, respectively.

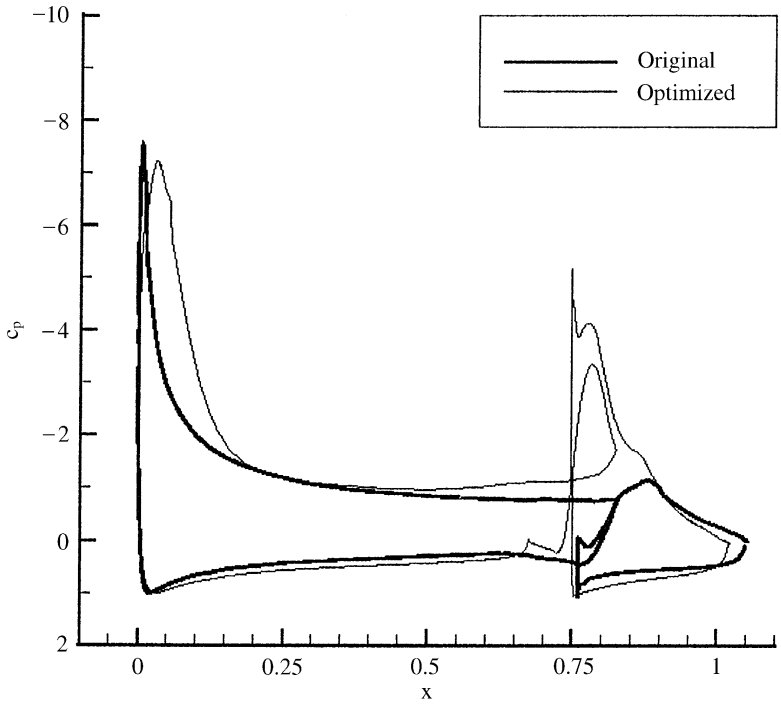

Fig. 10. c_p comparison for the application example 3.

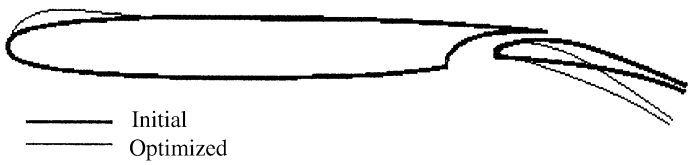

Fig. 11. Airfoil comparison for the application example 3.

The chosen airfoil has lift coefficient and pitching moment coefficient equal to 2.135 and -0.315 respectively, which correspond to 0.219 and 0.40 objective function values.

5.5. *Application example 4*: c_ℓ *maximization at* $M = 0.2$ *and* c_{dw} *reduction at* $M = 0.85$

The last example is related to a dual-point design solved through a multiobjective approach in which the first objective controls the lift coefficient in high lift, and the second one the wave drag coefficient in transonic cruise. The thickness constraint has been set at $t = 9.5\%$, no control is imposed on the pitching moment.

The modification functions operate on the whole airfoil, and the high-lift devices are modified following the blending method previously described.

The modification functions are the Hicks–Henne functions previously reported in Table 1, but with $x/c \in [0,1]$ and $\xi = x/c$, plus the ones reported in Table 2.

Table 2
Additional modification functions used in the application 4

Linear	Wagner
0.2ξ	$0.87\left(\frac{2\arcsin(\sqrt{\xi}) + \sin(2\arcsin(\sqrt{\xi}))}{\pi} - \xi\right)$
	$0.24\left(\frac{\sin(2k\arcsin(\sqrt{\xi}))}{k\pi} + \frac{\sin(2(k-1)\arcsin(\sqrt{\xi}))}{\pi} \quad k = 2, \ldots, 6\right)$
Polynomial	**Rear loading**
$0.52(0.5\xi^3 - 1.5\xi^2 + \xi)$	$6\,625\,000(1-\xi)\xi^{15}e^{1/5-20\xi}$
$0.4(\xi - \xi^2)$	$17\,500\,000(1-\xi)\xi^{18}e^{1/4-20\xi}$
$0.52(0.5\xi - 0.5\xi^3)$	$44\,440\,000(1-\xi)\xi^{22.66}e^{7/20-20\xi}$
	$90\,000\,000(1-\xi)\xi^{30}e^{1/2-20\xi}$

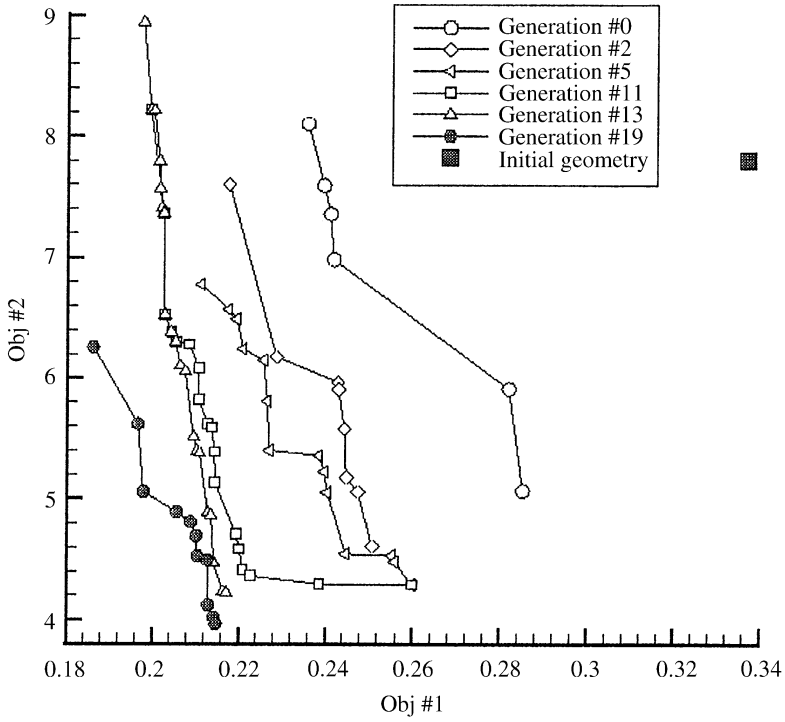

Fig. 12. Final and intermediate fronts related to the application example 4.

Linear, Hicks–Henne and Wagner functions are used to modify both upper and lower airfoil surface, so two design variables correspond to each function; polynomial functions work only on upper surface and rear loading only on lower surface.

A population of 40 individuals evolved for 20 generations; 8 bits were used for variable encoding; mutation at bit level with a probability of 2% and extended intermediate crossover

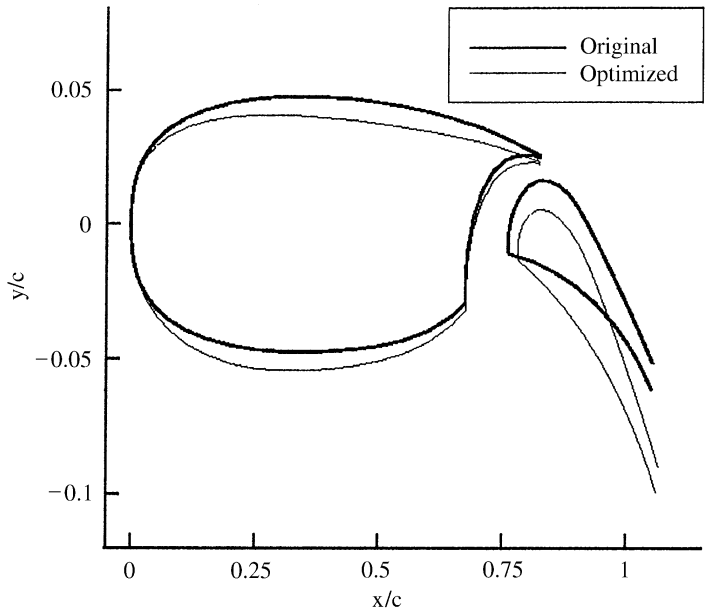

Fig. 13. Open-airfoil configuration comparison for the dual design point problem.

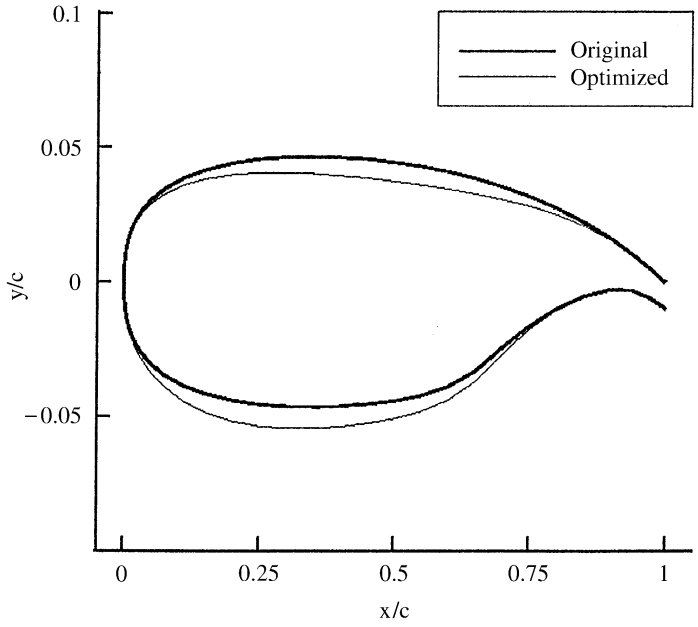

Fig. 14. Closed-airfoil configuration comparison for the dual design point problem.

with 100% activation probability were used. Fig. 12 reports the final Pareto front and some intermediate ones. The airfoil of the final front with better transonic performance was chosen. Figs. 13 and 14 report its shape, along with the initial one, in the open and closed configurations. The ordinate scale is enlarged in order to allow a better

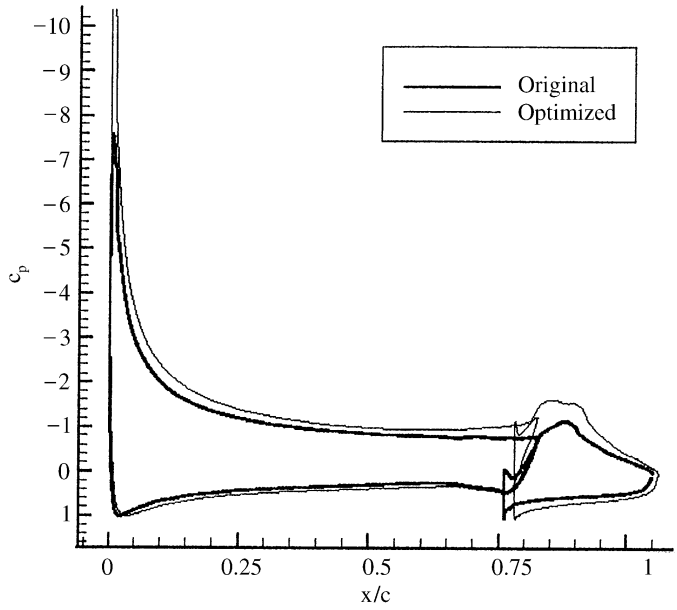

Fig. 15. High-lift c_p comparison for the dual design point problem.

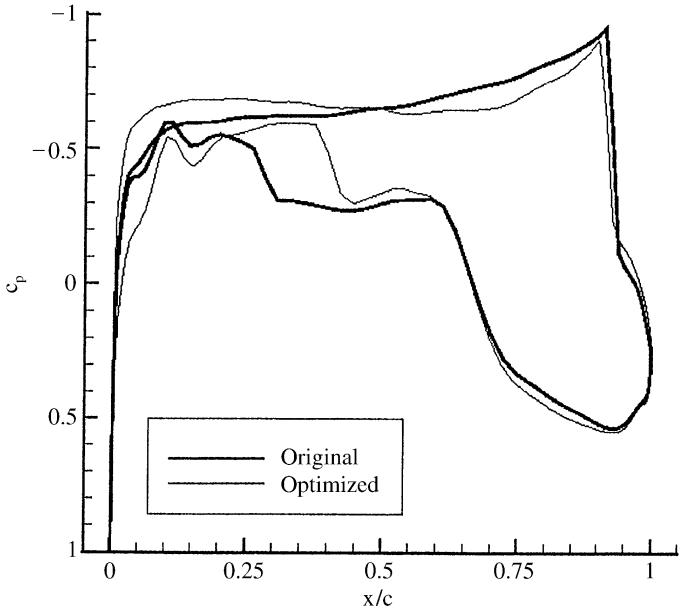

Fig. 16. Transonic cruise c_p comparison for the dual design point problem.

comparison. Figs. 15 and 16, finally, report the pressure distribution comparisons for the two design points.

For this airfoil, the lift coefficient c_ℓ is equal to 2.18 in the first design point, while the wave drag coefficient c_{dw} in the second design point is equal to 0.0099.

6. Conclusion

A numerical optimization tool for the aerodynamic design of single and multicomponent airfoils has been described. The applications illustrated regard both the single-point design of a high lift system and a dual-point design where the transonic cruise requirements are also simultaneously considered. The optimization system has generally shown good robustness and optimization capabilities. In particular, the geometry modification scheme introduced allows an easy and coherent modification of multielement airfoils.

The robustness characteristics of the multiobjective genetic algorithm are very useful for the optimization of high lift flows. In fact, in this type of working conditions the flow field solver may fail for many reasons and in ways that are not easily predictable, and therefore introduce noise in the fitness function; it is then very important to have an optimization procedure that can easily recover from these error.

Further work on the optimization procedure will be focused on the introduction of inverse and mixed design capabilities. Following this approach the design point could be specified either assigning a global goal, such as the maximization of lift, or a local one, such as the achievement of a specified pressure distribution on the whole airfoil or on a part of it. The capability of the genetic optimizer of dealing at the same time with discrete and continuous variables can also be conveniently used to solve design problems with varying topology and number of components of the high-lift system. Another field of possible improvements is the introduction of a hierarchical approach for the fitness evaluation. Following this idea, several solvers with different flow models and consequently different levels of accuracy can be used for the evaluation of the fitness, in order to restrict the use of the more computationally expensive models only when really needed.

References

[1] A.M.O. Smith, High-lift aerodynamics, J. Aircraft 12 (6) (1975) 501–530.
[2] W.K. Anderson, D.L. Bonhaus, R.J. McGhee, B.S. Walker, Navier-Stokes computations and experimental comparisons for multielement airfoil configuration, J. Aircraft 32 (6) (1995) 1246–1253.
[3] D. Quagliarella, Genetic algorithms applications in computational fluid dynamics, in: G. Winter, J. Periaux, Wiley, England, 1995, pp. 417–442.
[4] A. Vicini, D. Quagliarella, Airfoil and wing design through hybrid optimization strategies, AIAA J. 37 (5) (1999) 634–641.
[5] D.E. Goldberg, Genetic Algorithms in Search, Optimization and Machine Learning, Addison-Wesley, Reading, MA, 1989.
[6] A. Vicini, D. Quagliarella, Inverse and direct airfoil design using a multiobjective genetic algorithm, AIAA J. 35 (9) (1997) 1499–1505.
[7] D.P. Coiro, M. Amato, P. de Matteis, Numerical predictions of transonic viscous flows around aerofoils through and Euler/boundary layer interaction method, Aeronaut. J. Roy. Aeronaut. Soc. April (4) (1992) 157–165.
[8] A. Jameson, W. Schmidt, E. Turkel, Numerical solution of the Euler equations by finite volume methods using Runge-Kutta time-stepping schemes, AIAA Paper 81-1259, June 1981.
[9] M.J. Lightmill, On displacement thichness, J. Fluid Mech. part 4, 4 (1958) 661–663.

[10] E. Omar, T. Zierten, M. Hahn, E. Szpiro, A. Mahal, Two-dimensional Wind Tunnel Tests of a NASA Supercritical Airfoil with Various High Lift Systems — Vol. II. Test Data, The Boeing Company, Commercial Airplane Group.
[11] D. Quagliarella, A. Vicini, Coupling Genetic Algorithms and Gradient Based Optimization Techniques, in: D. Quagliarella et al. (Eds.), Genetic Algorithms and Evolution Strategies in Engineering and Computer Science, Wiley, England, 1997, pp. 289–309.